HHS Public Access

Author manuscript

J Am Chem Soc. Author manuscript; available in PMC 2019 July 25.

Published in final edited form as:

J Am Chem Soc. 2019 July 10; 141(27): 10736–10743. doi:10.1021/jacs.9b03661.

Chloride Control of the Mechanism of Human Ceruloplasmin Catalysis

Shiliang Tian[1], **Stephen M. Jones**[1], **Anex Jose**[1], **Edward I. Solomon**[1,*]

[1]Department of Chemistry, Stanford University, Stanford, California 94305, United States

Abstract

Unraveling the mechanism of ceruloplasmin (Cp) is fundamentally important towards understanding the pathogenesis of metal-mediated diseases and metal neurotoxicity. Here we report that Cl^-, the most abundant anion in blood plasma, is a key component of Cp catalysis. Based on detailed spectroscopic analyses, Cl^- preferentially interacts with the partially reduced trinuclear Cu cluster (TNC) in Cp under physiological conditions and shifts the electron equilibrium distribution among the two redox active type 1 (T1) Cu sites and the TNC. This shift in potential enables the intramolecular electron transfer (IET) from the T1 Cu to the native intermediate (NI) and accelerates the IET from the T1 Cu to the TNC, resulting in faster turnover in Cp catalysis.

Graphical Abstract

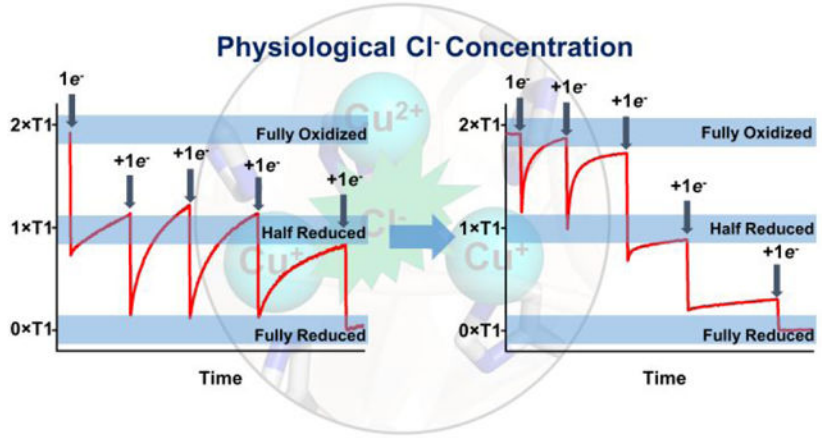

Introduction

Human serum Cp is a glycoprotein that binds up to 95% of the circulating copper in serum.[1] Cp is an essential ferroxidase critical for iron homeostasis,[2–3] and is closely associated with metal-mediated diseases and metal neurotoxicity. A neurodegenerative disorder resembling

* solomone@stanford.edu.

Supporting Information

This material is available free of charge via the Internet at http://pubs.acs.org.

Additional EPR, CD and MCD spectra, poised redox titration, stopped-flow kinetics and the simulation of steady-state kinetics.

Parkinson's disease has been related to very low Cp levels circulating in serum.[4] Mutations in the Cp gene lead to excess Fe accumulation in pancreas, retina and brain.[5–8] Studies of the mutational disease aceruloplasminemia reveal that Cp promotes efficient Fe efflux such that individuals lacking Cp develop oxidative injury secondary to Fe accumulation and significant neuronal damage.[9-10]

Structrually, Cp belongs to a large class of copper-containing enzymes called the multicopper oxidases (MCOs), which couple the one-electron oxidation of various substrates with the four-electron reduction of O_2 to H_2O.[11–12] The catalytic motif shared among all MCOs includes a minimum of four copper ions, arranged as a mononuclear T1 Cu site, which is the entry point of electrons from the substrates, and a TNC, which accepts the electrons from the T1 Cu via a Cys-His pathway and utilizes these in the four-electron reduction of O_2 (Figure 1a).[11–12] In the resting enzyme, the TNC is composed of a binuclear type 3 (T3) Cu pair that is antiferromagnetically coupled by an OH^- bridge and a non-bridged type 2 (T2) Cu that is ~ 3.5 A away from the T3 Cu (Figure 1a).[12] Traditional three-domain MCOs and the recently discovered two-domain small laccases all harbor four Cu ions.[13–14] A fundamental understanding of the catalytic cycle of traditional MCOs has been established by the study of *Rhus vernicifera* laccase (*Rv*L), a typical three-domain MCO.[15] On the other hand, Cp consists of six domains and contains six Cu ions arranged as three T1 Cu sites and a TNC (Figure 1b), which makes it a unique and the most complex MCO. The TNC is located at the interface of domains 1 and 6 and each of the T1Cu is coordinated to a cysteine and two histidine residues from domains 2, 4 and 6. The T1 Cu in domain 6 is coupled to the TNC via a Cys-His pathway similar to other MCOs. The second T1 Cu in domain 4 is 17 A away (Figure 1b) but can rapidly transfer its electron to the first T1 Cu.[16] T1Cu in domain 2, in which the axial methionine is replaced by a leucine residue, has a high potential (> 1 V) and appears to remain reduced during turnover.[17] The mechanistic picture of Cp is complicated by the presence of the two additional T1 Cu sites, and consequently far from being understood. Here we report the effects of Cl^-, the most abundant anion present in blood plasma (~ 100 mM),[18] on the human Cp catalytic mechanism. Based on spectroscopic analyses, we identify that Cl^- preferentially interacts with a partially reduced TNC, resulting in an electron redistribution among the copper sites reflecting a change in reduction potentials that greatly impacts the catalytic steps. The results are well aligned with the functional properties of the protein in Fe metabolic processes.

Results and Discussion

Reduction Titrations of Cp without Cl^-.

Anaerobic reduction titrations of fully oxidized Cp in the absence and presence of Cl^- were performed with stoichiometric additions of Fe(II) as the reductant (Figure 2), which has an affinity constant of at least 1×10^5 M^{-1} and transfers its electron completely to the T1 Cu at a rate of > 1200 s^{-1}.[19] The total number of oxidized T1 Cu was quantified by the intensity of its S(Cys)⟶Cu ligand to metal charge transfer (LMCT) band at 610 nm. In the absence of Cl^-, the intensity of the 610 nm band decreased by half upon addition of 1 equivalent Fe(II) (Figure 2a), indicating that 50 % of the two redox active T1 Cu sites were reduced (equally distributed, *vide infra).* The one-electron reduced T1 Cu sites essentially remained at the

same oxidation state after extended time, indicating there is no significant intramolecular electron transfer (IET) from the T1 Cu to the TNC. This observation is consistent with previous studies showing that only ~50 % of the T1 Cu was reoxidized when fully reduced (FR) Cp was reacted with O_2.[16, 20–21] The phenomenon indicated that the reduction potential of the T1 Cu sites is higher than those of the T2 and T3 Cu sites of the TNC in the absence of Cl^-.

Addition of a second equivalent of Fe(II) initially reduced the remaining T1 Cu within seconds, but the fully reduced 2×T1 state slowly reoxidized to the 1/2(2×T1) reduced state under anaerobic conditions, indicating that a one-electron IET from the fully reduced T1 Cu's to the TNC had occurred (Figure 2a). Notably, no significant further oxidation of the one-electron reduced T1 Cu sites was observed. Upon addition of a third equivalent of Fe(II) (Figure 2a), complete T1 reduction and re-oxidation back to the one- electron reduced state was again observed, corroborating that the IET from the T1 Cu sites to the TNC in the absence of Cl^- only occurs when both of the T1 Cu sites are reduced and then only one electron is transferred. Addition of a fourth equivalent of Fe(II) again reduced the remaining T1 Cu, followed by IET to the TNC which is fully reduced at this stage. Finally the T1 Cu sites became fully reduced upon the addition of a fifth equivalent of Fe(II).

To further investigate the electron distribution in partially reduced Cp, EPR spectra were also collected after the addition of l to 4 equivalents of Fe(II) (Figure S2). Intensities of the T1 and T2 Cu EPR features were used to determine the fraction of each Cu site in the oxidized state (Note: the T1 Cu fraction quantified by EPR at liquid N_2 temperature is equivalent to T1 Cu fraction quantified by the absorption spectrum at room temperature). The number of non-EPR-active reduced T3 Cu (Note: T3 functions as a $2e^-$ acceptor) was determined from the quantitative difference between the Fe(II) added and T1 and T2 Cu reduced. As shown in Figure S2 and Table S1, the amount of T1 Cu sites in the oxidized state was quantified to be 1.3, 1.1, 0.89 and 0.65, respectively upon the addition of 1 to 4 equivalents of Fe(II) and allowing for IET (after 30 min), consistent with the UV-Vis spectra (Figure 2a) indicating that half of the T1 Cu sites were first reduced and that IET mainly occurred from the fully reduced 2×T1 Cu to TNC. Moreover, both T1 Cu features diminished to the same extent upon additions of Fe(II), indicating that both T1 Cu sites have equivalent reduction potentials in the absence of Cl^-.[16] Upon addition of 3 equivalents of Fe(II) the EPR spectrum revealed that most of the T3 Cu was reduced but a majority of the T2 Cu remained oxidized (Figure S2c), indicating that the reduction potential of T3 Cu is higher than that of the T2 Cu center. Thus, the reduction potential order is **T1A Cu = T1B Cu > T3 Cu > T2 Cu** in the absence of Cl^-. Application of the Nernst equation to the T1 Cu pair indicates a reduction potential shift of −28 mV between the $^1/_2$(2×T1) reduced state and the 2×T1 reduced state. Our observation that the shift was sufficient to drive the IET from the T1 Cu pair to the TNC indicated that the reduction potential difference between the TNC (T2 and T3 Cu sites) and the T1 Cu pair is within ~30 mV.

Reduction Titrations of Cp with Cl^-.

To probe the effect of Cl^- on Cp reduction, the same set of experiments was performed in the presence of 100 mM NaCl, the physiologically relevant concentration.[18] Upon addition

of 1 equivalent of Fe(II), half of the two T1 Cu sites was reduced first, similar to the behavior in the absence of Cl^-. However, contrary to what was observed in the Cl^- free condition, the one-electron reduced T1 Cu pair transferred an electron to the TNC and regenerated the fully oxidized T1 Cu pair (Figure 2b). A similar process was observed after the addition of a second equivalent of Fe(II) (Figure 2b). EPR spectra of Cp after the addition of these initial two equivalents of Fe(II) and allowing for IET, showed no obvious reduction of the T1 or T2 Cu sites (Figure S3a and S3b), corroborating the UV-Vis results and implying the full reduction of the T3 Cu pair. Addition of a third equivalent of Fe(II) reduced half of the T1 Cu intensity from both UV-Vis in Figure 2b and EPR in Figure S3c. However, the relative intensities of the two T1 Cu sites (which can be distinguished based on slightly different EPR signals) diverged at this point (Figure S3c), indicating that the two T1 Cu sites in the presence of Cl^- have different potentials. After the addition of the fourth equivalent of Fe(II), over 60% of the T2 Cu was still oxidized in the presence of Cl^- (Figure S3d), while most of the T2 Cu was reduced in the absence of Cl^- (Figure S2d). These results revealed that a physiologically relevant concentration of Cl^- dramatically altered the relative reduction potentials of the Cu sites and led to the order: **T3 Cu >> T1B Cu >T1A Cu > T2 Cu**.

Reduction Potentials.

The potentials of T1 Cu sites both in the absence and presence of Cl^- (at a physiological concentration) were determined by poised potential titration (Table 1 and Figure S4). In the absence of Cl^-, both T1 Cu sites had the equivalent potential, quantified to be 429 ± 7 mV (Figure S4). In the 100 mM NaCl containing buffer, the average potential of the two T1 Cu sites was determined to be 421 ± 5 mV (Figure S4). However in the presence of Cl^-, the T1B Cu was selectively reduced over the T1A Cu upon addition of 3 equivalents of Fe(II) (T1A and T1B defined in Figure 3a). EPR spectral simulations revealed that 78% of T1A and 22% of T1B were in oxidized state, yielding a 65mV difference in reduction potential between the two T1 sites.

This was also supported by resonance Raman spectroscopy (rR). The rR spectra of fully oxidized Cp displayed bands at 340, 361, 380, 398, 411 and 425 cm^{-1} (Figure 4a), comparable to previously reported features,[22] where the intensity weighted average energies reflect the Cu-S stretching modes of two T1 Cu sites. In the absence of Cl^-, Fe(II) addition led to an intensity decrease of all the rR bands to the same extent (Figure 4a), consistent with both T1 Cu sites having the same potential, while in the presence of Cl^- the three rR bands at 361, 398 and 411 cm^{-1} selectively decreased upon the addition of 3 equivalents of Fe(II) (Figure 4b), corroborating the non-equivalence of the two T1 Cu sites in the presence of Cl^- as demonstrated by EPR (Figure 3A). The potentials of the T2 and T3 Cu sites in Table 1 were obtained by reduction titration monitored by EPR and spectrum fitting with the Nernst equation assuming the Cu sites were in equilibrium with each other (Figure S2 and Figure S3).

Spectroscopic Evidence of Cl^- Binding.

From Table 1, the presence of Cl^- in the buffer increased the potential of the T3 Cu by ~ 100 mV and decreased that of the T2 Cu by ~60 mV, pointing to the possibility of Cl^- binding to

the partially reduced TNC. To evaluate this possibility, UV-Vis, EPR and MCD spectra of Cp in different oxidation states in buffers without and with Cl^- were compared. For fully oxidized Cp, no significant difference was observed upon Cl^- addition (Figure S5). However, in the EPR spectra of the partially reduced TNC (by 3 equivalents of Fe) in the presence of Cl^-, the lowest field parallel hyperfine line of the T2 Cu at 2725 G shifted up-field by ~20 G (Figure 3a), indicating a change in the electronic structure of the TNC. The MCD spectrum of fully oxidized Cp did not change upon addition of Cl^- (Figure S5c). For the partially reduced Cp (by $3e^-$), the MCD spectrum without Cl^- displayed weak negative bands at 21700 cm^{-1} and 23800 cm^{-1}, an intense negative band at 14350 cm^{-1} and a weak positive band at 12750 cm^{-1} (Figure 3b), similar to the spectra of fully oxidized Cp in Figure S5c. The bands at 12750 cm^{-1}, 21700 cm^{-1} and 23800 cm^{-1} have been assigned as the T2 Cu ligand field transition, $OH^- \pi \rightarrow$ T2 Cu and His $\pi \rightarrow$ T2 Cu charge transfer transitions, respectively.[23] Addition of Cl^- at this $3e^-$ reduced state of Cp induced the changes of these MCD bands (Figure 3b), featuring weak positive bands at 21200 cm^{-1} and 23700 cm^{-1} and a negative band at 12100 cm^{-1}, corroborating the electronic structural changes at the TNC observed in EPR. Hence, the changes in the EPR and MCD spectra are ascribed to a perturbation of oxidized T2 Cu due to Cl^- binding to the TNC upon reduction of the T3 Cu pair. A geometry optimized structure of Cl^- bound to the partially reduced TNC was generated by DFT calculations (Figure S6). The Cl^- is calculated to bridge between the T2 Cu site and one of the T3 Cu atoms with bond lengths of 2.4 A and 2.8 A, respectively but is further away from the other T3 Cu (~ 4.3 A). The geometry of the T2 Cu site changed from T-shaped to square-planar which would increase the energy of the d_{x2-y2} orbital and result in the smaller $g_{//}$ value observed experimentally (the $g_{//}$ changes from 2.24 to 2.22 upon Cl^- binding).

The rR spectrum, which is sensitive to the perturbation of the T1 Cu coordination environment, showed no energy shift in going from the resting to the T3 reduced and in adding Cl^- to both (Figure S7), indicating no significant structural change of the T1 Cu sites. The possible effect of an ionic strength change induced by the NaCl was evaluated by collecting EPR spectra of the three-electron reduced Cp under three buffer conditions: MOPS only, MOPS with NaCl, and MOPS with Na_2SO_4 matching the ionic strength of the second buffer (Figure S8). The EPR features of the T1 Cu sites remained the same between the MOPS only and MOPS-Na_2SO_4 buffer, but re-distributed due to the T1 Cu potential difference in the MOPS-NaCl buffer, excluding the involvement of ionic strength in the observed Cl^- effect. The elimination of Cl^- binding to T1Cu and an ionic strength effect suggest that the T1B Cu reduction potential increase reflects its perturbation by the Cl^- binding to the partially reduced TNC via the Cys-His pathway (i.e. an allosteric effect).[24] The decrease in the reduction potential of T1A Cu likely reflects a local Cl^- binding site, which would electrostatically lower its reduction potential. Indeed, the perturbation of T1 Cu sites in Cp with anions addition has been reported.[25–26]

Single Turnover Kinetics of Cp without and with Cl^-.

The molecular mechanism of MCOs based on *RvL* studies is shown in Figure 5a. When the fully reduced MCO reacts with O_2, two key intermediates are formed in the reductive cleavage of the O-O bond by the TNC: the peroxy intermediate (PI)[27] where O_2 is reduced

by two electrons, and the native intermediate (NI),[28] in which O_2 is fully reduced to the water level . In the absence of reductant, NI in RvL decays to the resting oxidized (RO) form with a rate (~ 6.6×10^{-3} s^{-1}at 4 °C and ~ 0.05 s^{-1} at 25 °C),[28] much slower than the turnover rate(> 560 s^{-1} at 25 °C), and thus this process is not catalytically relevant.[29] Alternatively, in the presence of reductant, NI is rapidly reduced directly to the fully reduced form (> 700 s^{-1}at 4 °C).[30] Therefore, NI is the catalytically relevant fully oxidized form and is rapidly reduced in the catalytic cycle.

We expanded these mechanistic studies to Cp and in particular evaluated the effect of physiologically relevant Cl^- on Cp catalysis. The kinetics of the reaction of fully reduced Cp with O_2 were measured by stopped-flow absorption under different O_2 concentrations (Figure S9 and S10). Without or with Cl^-, fully reduced Cp reacted with O_2 with rates of ~2 × 10^6 M^{-1} s^{-1}, comparable to *Rv*L[27] The IET from T1 Cu to PI in Cp was too fast to measure (> 1500 s^{-1}), effectively resulting in the four-electron reduction of O_2 in one step. NI in Cp was trapped by rapid freeze quench (RFQ) and characterized by EPR (Figure S11). The same EPR spectrum of NI was observed in the absence and presence of Cl^-, featuring a broad fast relaxing signal below 2.0 (g ~ 1.9) similar to the g ~ 1.65 feature of NI in *Rv*L.[28] Consistent with previous findings in *Rv*L,[28] the g ~ 1.9 signal could be detected only at low temperature (< 20 K) and high power (> 0.1 mW).

However, NI in Cp decayed back to RO at a rate of ~ 0.50 s^{-1} with or without Cl^- (Figure S11), which is two orders of magnitude faster than the NI decay rate in *Rv*L (~ 6.6×10^{-3} s^{-1}).[28] The IET rate between the T1 Cu site and NI in Cp was measured using Fe(II) as the reductant, as it rapidly reduced the T1 Cu (> 1200 s^{-1}).[19] In the absence of Cl^-, no IET from the T1 Cu to the TNC was observed before the complete decay of NI to RO (Figure S12), while in the presence of Cl^- the IET from the T1 Cu site to NI proceeded with a rate of ~ 0.60 s^{-1} (Figure 5b), which is comparable to the decay rate of NI to RO (~ 0.50 s^{-1}) but three orders of magnitude slower than the NI reduction rate in RvL (> 700 s^{-1}).[30] The IET from the T1 Cu to the TNC in the RO form of Cp was also measured and determined to be ~ 1.2×10^{-3} s^{-1} and ~ 6.6×10^{-3} s^{-1} in the absence and presence of Cl^-, respectively (Figure S13). Overall, the presence of Cl^- did not affect NI formation upon O-O bond cleavage but accelerated the IET from T1 Cu to TNC in RO reduction and enabled the IET from the T1 Cu to NI in Cp catalysis.

Based on spectroscopic results above, the Cl^- accelerated IET rate in Cp appears to derive from the increased potentials of the TNC in the RO and NI states promoted by Cl^- binding to the partially reduced TNC. From Table 1, the driving forces for the IET from the T1 to T3 Cu are ~20 mV without Cl^- and ~100 mV with Cl^-. The Marcus equation was then employed to compute the T1 to TNC IET rate ratio.[31] The rate was calculated to be accelerated by a factor of ~5 in the presence of Cl^- assuming the same reorganization energies (λ) and electronic-coupling matrix elements (H_{DA}) (Table S2). This is consistent with our experimental values that the T1 Cu to RO IET rates were 0.0012 s^{-1} and 0.0066 s^{-1} without and with Cl^-, respectively. This approach was also used to evaluate the IET rate difference from the T1 Cu to NI relative to RO in the presence of Cl^-. Using past results that the reorganization energy of RO is 0.3 eV larger than that of NI and the driving force for NI reduction is 7 kcal/mol higher than that of RO due to the strong proton affinity of the μ_3-oxo

ligand in NI,[32] the IET rate to NI is calculated to be ~10^3 that of RO (Table S3), consistent with our experimental observation that NI is reduced at a rate of ~0.6 s^{-1} (Figure 5b) and RO at ~0.0009 s^{-1} at 4 °C (Figure S13f).

Cl^- Impact on the Steady-State Kinetics of Cp.

To correlate our single turnover kinetic results to enzymatic activities under physiologically relevant conditions, we measured the steady-state Cp oxidase activity without and with Cl^- at pH7.0 using *o*-dianisidine as a substrate (widely used in biological and clinical assays for Cp activity).[33–34] The k_{cat} at 25 °C in the presence of Cl^- was determined to be ~ 0.062 s^{-1}which is ten-fold faster than k_{cat} of ~ 0.0073 s^{-1} in the absence of Cl^- (Figures 6 and S14). This rate increase due to Cl^- is consistent with a previous qualitative observation in Cp catalyzed *p*-phenylenediamine oxidation.[35]

The steady-state kinetics of Cp were simulated using the mechanistic model of *RvL* in Figure 5a and reaction rates obtained from the single turnover kinetics of Cp (Figure S15a). The simulated steady-state rates in the presence of Cl^- were ~ 0.058 s^{-1} at 25 °C and ~ 0.0079 s^{-1} at 4 °C, matching the experimental results of ~ 0.062 and ~ 0.008 s^{-1} respectively (Figure S15b). The simulated steady-state rate in the absence of Cl^- was ~ 0.0049 s^{-1} at 25 °C, comparable to the experimental result of ~ 0.0073 s^{-1}. The simulated speciation revealed that the major species present at steady-state in the presence of Cl^- is RO (> 99.8%, Figure S15c), substantiating the involvement of RO reduction in Cp catalysis. The simulated flux rates at the steady-state revealed that both RO and NI reduction contribute to the formation of fully reduced (FR) Cp at rates of ~ 0.0066 and 0.0079 s^{-1} respectively at 25 °C (Figure S15c), indicating the IET from T1 Cu to the TNC during RO and NI reduction both contribute to the rate determining step in Cp catalysis. The Cl^- enabled IET from the T1 Cu to NI opens up a second catalytic cycle (FR → PI → NI → FR) in addition to the FR → PI → NI → RO → FR cycle present in the Cl^- free condition. Consequently, the FR formation rate is increased two-fold, which in combination with Cl^- promoted five-fold increase in the rate of RO reduction (Figure 5a) results in the ten-fold increase in the overall turnover frequency compared to the Cl^- free condition.

The ferroxidase activity of Cp has been reported in the literature but with contradictory values (~ 1 s^{-1} vs ~ 0.1 s^{-1}) at pH 7.0 and with no Cl^- effect on the lower reported rate.[26, 36] We reevaluated this Cp activity by quantifying the rate of ferric ion absorbance increase at 315 nm vs the concentration of Cp (Figure S16).[37–38] The rates obtained were 0.8 ± 0.1 s^{-1} and 1.2 ± 0.2 s^{-1} in the absence and presence of Cl^- respectively, which is consistent with one of the previous reports (~ 1 s^{-1} in the presence of Cl^-).[36] Notably, this ferrous oxidation rate in the ferroxidase assay (~ 1 s^{-1}) is two orders of magnitude faster than the T1 Cu to TNC IET rate (~ 0.01 s^{-1}) in Cp. This fast turnover rate precludes the involvement of the T1Cu to TNC IET process in the catalytic cycle of this assay, suggesting an alternative direct ET path from the ferrous ion to the TNC under these in vitro conditions. See the supporting information (Figure S17 and S18) for further detail on an additional Fe(II) binding site.

Conclusions

In summary, these spectroscopic and kinetic studies show that Cl^- under physiologically relevant conditions is bound to the partially reduced TNC (T3 reduced and T2 oxidized) in Cp. This increases the reduction potential of the TNC in both the RO and NI states. These thermodynamic changes accelerate the IET from the T1 Cu to the TNC in the reduction of RO and enable IET from the T1 Cu to NI in Cp catalysis, which opens up a second catalytic cycle (FR → PI → NI → FR) in addition to the FR → PI → NI → RO → FR cycle present under the Cl^- free condition. Together these result in an order of magnitude faster turnover of Cp compared to the Cl^- free condition. Finally, the fast NI decay and slow NI reduction in Cp lead to a change in the rate determining step in Figure 5a with the involvement of RO reduction in Cp catalysis and result in the orders of magnitude slower turnover rate of Cp (< 0.1 s^{-1}) compared to *Rv*L (> 560 s^{-1}).[29]

Experimental Section

General.—All chemicals were purchased from Sigma-Aldrich and used without further purification. Water was purified on a Nanopure Diamond purifier from Barnstead to a resistivity of > 17 MΩ cm.

Human Cp Purification and Characterization.—Fresh human plasma is readily available from the Stanford Blood Center, and Cp is purified from this by the previously reported rapid one-step method with a yield of ~ 20 mg/deciliter.[16–17] The purified Cp was oxidized with 20 equivalent of H_2O_2 to achieve its fully oxidized form and the excess H_2O_2 was removed by PD-10 desalting column. The quality and function of the human Cp have been assessed by UV-vis, EPR and biquinoline assay (6.3 ± 0.1 Cu ions per Cp).

Ultraviolet-visible spectroscopy (UV-vis).—UV-vis spectra were recorded on a Hewlett-Packard HP8452A diode array UV-vis spectrophotometer in a 1 cm path length cuvette.

Stopped-flow Kinetics.—Stopped-flow data were obtained using an Applied Photophysics SX.19 stopped- flow absorption spectrophotometer equipped with a Hg/Xe Arc lamp and a PDA1 photodiode array detector in a purge box (Cleatech Isolation Glove Box 2100) equipped with an oxygen sensor (Neutronics Model 1100). Stopped-flow experiments were conducted at 4 °C maintained using a water/ethanol temperature bath (Fisher Scientific Isotemp 3016) with a cell path length of 1 cm. All solutions were freshly prepared in an anaerobic glovebox. Both injector ports of the stopped-flow were degassed with ~ 3.0 mM sodium dithionite for ~ 20 min and then washed with the degassed buffer thoroughly. The protein samples were loaded on the stopped-flow at concentrations of ~ 50 μM.

Electron Paramagnetic Resonance (EPR).—X-band EPR spectra were obtained with a Bruker EMX spectrometer, an ER 041 XG microwave bridge, and an ER4119HS or and ER4116DM resonator. Sample temperatures from 77–100 K are maintained using a liquid nitrogen finger dewar. Temperatures on the order of 3.5–77 K are achieved using an ITC5 03

temperature controller with an ESR900 Continuous Flow Cryostat. The X-band EPR parameters were as follows: Freq. ≈ 9.6 GHz, Power ≈ 2 mW, Rec. gain = 30, Mod. Freq. = 100 kHz, Mod. Amp. = 4.00 G. EPR spin quantitation of the paramagnetic copper content was performed using a 1.0 mM standard solution of $CuSO_4 \cdot 5H_2O$, 2 mM HCl, and 2 M $NaClO_4$. EPR simulations were performed using the EasySpin software package.[39]

Resonance Raman (rR).—rR samples were excited at 647.1 nm using a Coherent I90C-K Kr+ ion laser while the sample was immersed in a liquid nitrogen cooled (77 K) EPR finger dewar (Wilmad). Power was ~40 mW at the sample. Data were recorded for 20 minutes while rotating the sample to minimize photodecomposition. The spectra were recorded using a Spex 1877 CP triple monochromator with a 1200 groves/mm holographic spectrograph grating, and detected by an Andor iDus CCD cooled to −80 °C. Spectra were calibrated on the energy axis to citric acid.

Circular Dichroism (CD).—CD data in the near-IR (600 – 2000 nm) were collected on a Jasco spectropolarimeter (J730) operating with a liquid N_2-cooled InSb detector.

Magnetic Circular Dichroism (MCD).—MCD spectra in the UV-Vis (300nm-900nm) were collected on a Jasco J810 with an S20 PMT detector. The magnetic field was supplied by an Oxford SM4000 7 T superconducting magnetooptical dewar. The sample temperature was measured with a calibrated Cernox resistor (Lakeshore Cryogenics) inserted into the MCD cell. The MCD sample cells consisted of two quartz disks with a 3-mm rubber spacer, and protein samples for MCD contained ~60 vol% of glycerol in order to form an optical-quality glass upon freezing. The data were corrected for zero-field baseline effects induced by cracks in the glass by subtracting the corresponding 0 T scan.

Rapid-freeze-quench (RFQ).—RFQ-EPR samples were prepared by mixing a 0.4 mM fully reduced Cp solution with an oxygen saturated buffer solution (~ 2.0 mM O_2) at 4 °C using Kintek Quench-Flow Apparatus Model RFQ-3. The sample was frozen by spraying into approximately −130 °C spectrophotometric grade isopentane in a Pyrex collection funnel attached to the EPR tube. Pre-cooled packing rods and long needles were used for packing the frozen powder into the base of the EPR tube while being maintained at −130 °C. After packing, the samples were transferred to a Dewar containing liquid nitrogen and stored until collection of the EPR spectra.

Reduction Potential Determinations.—Absolute reduction potentials of the T1 Cu were obtained by the poised potential method reported previously.[16] 40 μl of degassed 500 mM $K_3[Fe(CN)_6]$ stock solution was added to a 2000 μl solution of degassed 10 μM fully oxidized Cp in a 1cm path length anaerobic cuvette with a Teflon stopcock to yield a final concentration of 10 mM $K_3[Fe(CN)_6]$. A small quantity of a concentrated stock solution of degassed K^[$Fe(CN)_6$] was added under stirring to yield a final concentration of 0.2, 0.5, 1.0, 2.0, 5.0, 10, 20 and 50 mM of K4[$Fe(CN)_6$] respectively. The absorption spectra were taken over time until the reaction was complete (> 30min). All sample handling was done in a glovebox. The redox potential of T2 and T3 Cu sites were obtained from the fitting of the reduction titrations with Nernst equation assuming each Cu site is in equilibrium with the other Cu sites. All the measurements were repeated three times to generate the error bars.

DFT calculation.—Geometry optimized structure of chloride bound to the partially reduced TNC performed using Gaussian 16 [40] The geometry optimization was performed using B3LYP functional with basis set TZVP for Cu and coordinated N/O, Cl atoms and TZV for the rest. The starting geometry of the TNC was adapted from the crystal structure of human serum ceruloplasmin (PDB: 2J5W, Res. 2.8 Å). To reflect the features of the crystal structure, the positions of α-C atoms that connected the side chains to the protein backbone were fixed. Three residues Tyr107, E112 and D995 forming hydrogen bonds to the coordinated His ligands were involved in the calculation.

Electron Transfer (ET) Rate Calculation.—In the context of Marcus theory first-order IET rates can be expressed in terms of the driving force (ΔG°), the reorganization energy (λ) and the electronic-coupling matrix element (H_{DA}), which reflects the ET pathway.[31] Defined by the Marcus Equation:

$$k_{ET} = \frac{2\pi}{\hbar\sqrt{4\pi\lambda kT}} H_{DA}^{2} \exp[-\frac{\left(\Delta G^{o} + \lambda\right)^{2}}{4\lambda kT}]$$

Rearrangement of the Marcus equation into ratio of ET rates (H_{DA} is assumed to be equivalent):

$$\frac{k_{ET1}}{k_{ET2}} = \sqrt{\frac{\lambda_2}{\lambda_1}} \exp\{\left[-\frac{\left(\Delta G_1^0 + \lambda_1\right)^2}{4\lambda_1 kT}\right] - \left[-\frac{\left(\Delta G_2^0 + \lambda_2\right)^2}{4\lambda_2 kT}\right]\}$$

The inner-sphere reorganization energies (λ_i) were computed as 1.2 eV for the native intermediate (NI) and 1.5 eV for the resting oxidized (RO) form.[32] The reorganization energy for the T1 Cu site is 0.6 – 0.8 eV.[41]

Cp Oxidase Activity with Chromogenic Substrate.—Cp oxidase activity was measured using *o*-dianisidine free base as a substrate.[33–34] Assays were performed at 25 °C or 4 °C with 0.18 μM fully oxidized Cp in 100 mM MOPS pH7.0 buffer or 25 mM MOPS pH7.0 buffer with 100 mM NaCl containing 19.5, 39.0, 65.0, 97.5, 130.0, 162.5, 195.0 or 227.5 μM *o*-dianisidine respectively. The rate of the reaction is defined as per electron per Cp per second (Note *o*-dianiside is a $2e^-$ donor), based on the extinction coefficient of the oxidized *o*-dianisidine at 500 nm, $\varepsilon_{500nm} = 4.83 \times 10^3\ M^{-1}cm^{-1}$.[34] All the reactions were repeated three times to generate the error bars. The reaction rates were plotted versus the *o*-dianisidine concentration and subsequently analyzed by direct fitting to the Michaelis-Menten equation using Origin 2019 software (OrginLab Corporation).

Cp Ferroxidase Activity.—Cp ferroxidase activity was measured using $(NH_4)Fe(SO_4)_2$ as a substrate.[37–38] Assays were performed at 25 °C in 100 mM MOPS pH7.0 buffer or 25 mM MOPS pH7.0 buffer with 100 mM NaCl. The absorption increase at 315 nm was monitored on the UV-Vis absorption spectra upon addition of 0.2 mM $(NH_4)Fe(SO_4)_2$ (added from a freshly anaerobically prepared 100 mM stock solution) to 2 ml air-saturated buffer containing 0, 0.25, 0.50, 0.75, 1.00 and 1.25 μM of Cp respectively. The absorption

difference of 2200 $M^{-1}cm^{-1}$ at 315 nm was used to determine the formation of Fe^{3+} per mole of Fe^{2+}.[37] The ferroxidase activity was determine by a linear fitting of Fe^{3+} formation rate vs Cp concentration. All the measurements were repeated three times to generate the error bars.

Supplementary Material

Refer to Web version on PubMed Central for supplementary material.

Acknowledgments

This research was supported by the National Institute of Health (NIH) Grant R01DK031450 (to E.I.S.) and Ruth L. Kirschstein National Research Service Award (NRSA) F32GM122174 (to S.T.).

References

1. Healy J; Tipton K, Ceruloplasmin and what it might do. J. Neural Transm. 2007, 114 (6), 777–781. [PubMed: 17406962]
2. Harris ZL; Takahashi Y; Miyajima H; Serizawa M; MacGillivray RT; Gitlin JD, Aceruloplasminemia: molecular characterization of this disorder of iron metabolism. Proc. Natl. Acad. Sci. U.S.A. 1995 92 (7), 2539–2543. [PubMed: 7708681]
3. Xu X; Pin S; Gathinji M; Fuchs R; Harris ZL, Aceruloplasminemia: An inherited neurodegenerative disease with impairment of iron homeostasis. Ann. N. Y. Acad. Sci. 2004, 1012, 299–305. [PubMed: 15105274]
4. Miyajima H; Nishimura Y; Mimguchi K; Sakamoto M; Shimizu T; Honda N, Familial apoceruloplasmin deficiency associated with blepharospasm and retinal degeneration. Neurology 1987, 37 (5), 761. [PubMed: 3574673]
5. Yoshida K; Furihata K; Takeda S. i.: Nakamura A; Yamamoto K; Morita H; Hiyamuta S; Ikeda S. i.; Shimizu N; Yanagisawa N, A mutation in the ceruloplasmin gene is associated with systemic hemosiderosis in humans. Nat. Genet. 1995, 9 (3), 267–272. [PubMed: 7539672]
6. Daimon M; Kato T; Kawanami T; Tominaga M; Igarashi M; Yamatani K; Sasaki H, A Nonsense Mutation of the Ceruloplasmin Gene in Hereditary Ceruloplasmin Deficiency with Diabetes Mellitus. Biochem. Biophys. Res. Commun. 1995, 217 (1), 89–95. [PubMed: 8526944]
7. Harris ZL; Migas MC; Hughes AE; Logan JI; Gitlin JD, Familial dementia due to a frameshift mutation in the caeruloplasmin gene. Q. J. Med. 1996, 89 (5), 355–360.
8. Okamoto N; Wada S; Oga T; Kawabata Y; Baba Y; Habu D; Takeda Z; Wada Y, Hereditary ceruloplasmin deficiency with hemosiderosis. Hum. Genet. 1996, 97 (6), 755–758. [PubMed: 8641692]
9. Yoshida K; Kaneko K; Miyajima H; Tokuda T; Nakamura A; Kato M; Ikeda S. i., Increased lipid peroxidation in the brains of aceruloplasminemia patients. J. Neurol. Sci. 2000, 175 (2), 91–95. [PubMed: 10831768]
10. Patel BN; Dunn RJ; Jeong SY; Zhu Q; Julien J-P; David S, Ceruloplasmin Regulates Iron Levels in the CNS and Prevents Free Radical Injury. J. Neurosci. 2002, 22 (15), 6578–6586. [PubMed: 12151537]
11. Solomon EI; Sundaram UM; Machonkin TE, Multicopper Oxidases and Oxygenases. Chem. Rev. 1996 96 (7), 2563–2606. [PubMed: 11848837]
12. Solomon EI; Heppner DE; Johnston EM; Ginsbach JW; Cirera J; Qayyum M; Kieber-Emmons MT; Kjaergaard CH; Hadt RG; Tian L, Copper Active Sites in Biology. Chem. Rev. 2014, 114 (7), 3659–3853. [PubMed: 24588098]
13. Zaitseva I; Zaitsev V; Card G; Moshkov K; Bax B; Ralph A; Lindley P, The X-ray structure of human serum ceruloplasmin at 3.1 Â: nature of the copper centres. J. Biol. Inorg. Chem. 1996, 1 (1), 15–23.

14. Zaitsev NV; Zaitseva I; Papiz M; Lindley FP, An X-ray crystallographic study of the binding sites of the azide inhibitor and organic substrates to ceruloplasmin, a multi-copper oxidase in the plasma. J. Biol. Inorg. Chem. 1999, 4 (5), 579–587. [PubMed: 10550686]
15. Solomon EI; Augustine AJ; Yoon J, O_2 Reduction to H_2O by the multicopper oxidases. Dalton Trans. 2008, (30), 3921–3932. [PubMed: 18648693]
16. Machonkin TE; Solomon EI, The Thermodynamics, Kinetics, and Molecular Mechanism of Intramolecular Electron Transfer in Human Ceruloplasmin. J. Am. Chem. Soc. 2000, 122 (50), 12547–12560.
17. Machonkin TE; Zhang HH; Hedman B; Hodgson KO; Solomon EI, Spectroscopic and Magnetic Studies of Human Ceruloplasmin: Identification of a Redox-Inactive Reduced Type 1 Copper Site. Biochemistry 1998, 37 (26), 9570–9578. [PubMed: 9649340]
18. Morrison G, Serum Chloride In Clinical Methods: The History, Physical, and Laboratory Examinations, 3rd ed.; Walker HK; Hall WD; Hurst JW, Eds. Butterworths: Boston, 1990.
19. Quintanar L; Gebhard M; Wang T-P; Kosman DJ; Solomon EI, Ferrous Binding to the Multicopper Oxidases Saccharomyces cerevisiae Fet3p and Human Ceruloplasmin: Contributions to Ferroxidase Activity. J. Am. Chem. Soc. 2004, 126 (21), 6579–6589. [PubMed: 15161286]
20. Carrico RJ; Malmström BG; Vänngård T, A Study of the Reduction and Oxidation of Human Ceruloplasmin. Eur. J. Biochem. 1971, 22 (1), 127–133. [PubMed: 5099210]
21. De Ley M; Osaki S, Intramolecular electron transport in human ferroxidase (caeruloplasmin). Biochem. J. 1975, 151 (3), 561–566. [PubMed: 1218091]
22. Tosi L; Garnier A; Herve M; Steinbuch M, Ceruloplasmin-anion interaction a resonance Raman spectroscopic study. Biochem. Biophys. Res. Commun. 1975, 65 (1), 100–106. [PubMed: 167763]
23. Quintanar L; Yoon J; Aznar CP; Palmer AE; Andersson KK; Britt RD; Solomon EI, Spectroscopic and Electronic Structure Studies of the Trinuclear Cu Cluster Active Site of the Multicopper Oxidase Laccase: Nature of Its Coordination Unsaturation. J. Am. Chem. Soc. 2005, 127 (40), 13832–13845. [PubMed: 16201804]
24. Augustine AJ; Kragh ME; Sarangi R; Fujii S; Liboiron BD; Stoj CS; Kosman DJ; Hodgson KO; Hedman B; Solomon EI, Spectroscopic Studies of Perturbed T1 Cu Sites in the Multicopper Oxidases Saccharomyces cerevisiae Fet3p and Rhus vernicifera Laccase: Allosteric Coupling between the T1 and Trinuclear Cu Sites. Biochemistry 2008, 47 (7), 2036–2045. [PubMed: 18197705]
25. Byers W; Curzon G; Garbett K; Speyer BE; Young SN; Williams RJP, Anion-binding and the state of copper in caeruloplasmin. Biochim. Biophys. Acta 1973, 310 (1), 38–50. [PubMed: 4351064]
26. Musci G; Bellenchi GC; Calabrese L, The multifunctional oxidase activity of ceruloplasmin as revealed by anion binding studies. Eur. J. Biochem. 1999, 265 (2), 589–597. [PubMed: 10504390]
27. Cole JL; Ballou DP; Solomon EI, Spectroscopic characterization of the peroxide intermediate in the reduction of dioxygen catalyzed by the multicopper oxidases. J. Am. Chem. Soc. 1991, 113 (22), 8544–8546.
28. Lee S-K; George SD; Antholine WE; Hedman B; Hodgson KO; Solomon EI, Nature of the Intermediate Formed in the Reduction of O_2 to H_2O at the Trinuclear Copper Cluster Active Site in Native Laccase. J. Am. Chem. Soc. 2002, 124 (21), 6180–6193. [PubMed: 12022853]
29. Petersen LC; Degn H, Steady-state kinetics of laccase from Rhus vernicifera. Biochim. Biophys. Acta 1978, 526 (1), 85–92. [PubMed: 150864]
30. Heppner DE; Kjaergaard CH; Solomon EI, Mechanism of the Reduction of the Native Intermediate in the Multicopper Oxidases: Insights into Rapid Intramolecular Electron Transfer in Turnover. J. Am. Chem. Soc. 2014, 136 (51), 17788–17801. [PubMed: 25490729]
31. Marcus RA; Sutin N, Electron transfers in chemistry and biology. Biochim. Biophys. Acta 1985, 811 (3), 265–322.
32. Heppner DE; Kjaergaard CH; Solomon EI, Molecular Origin of Rapid versus Slow Intramolecular Electron Transfer in the Catalytic Cycle of the Multicopper Oxidases. J. Am. Chem. Soc. 2013, 135 (33), 12212–12215. [PubMed: 23902255]
33. Brown MA; Stenberg LM; Mauk AG, Identification of catalytically important amino acids in human ceruloplasmin by site-directed mutagenesis. FEBS Lett. 2002, 520 (1–3), 8–12. [PubMed: 12044861]

34. Siotto M; Pasqualetti P; Marano M; Squitti R, Automation of o-dianisidine assay for ceruloplasmin activity analyses: usefulness of investigation in Wilson's disease and in hepatic encephalopathy. J. Neural Transm. 2014, 121 (10), 1281–1286. [PubMed: 24663495]

35. Musci G; Bonaccorsi di Patti MC; Calabrese L, Modulation of the redox state of the copper sites of human ceruloplasmin by chloride. J. Protein Chem. 1995, 14 (7), 611–619. [PubMed: 8561857]

36. Cortes L; Roberts BR; Wedd AG; Xiao Z, Molecular Aspects of a Robust Assay for Ferroxidase Function of Ceruloplasmin. Inorg. Chem. 2017, 56 (9), 5275–5284. [PubMed: 28414228]

37. Bonomi F; Kurtz DM Jr.; Cui X, Ferroxidase activity of recombinant Desulfovibrio vulgaris rubrerythrin. J. Biol. Inorg. Chem. 1996, 1 (1), 67–72.

38. Hassett RF; Yuan DS; Kosman DJ, Spectral and Kinetic Properties of the Fet3 Protein from Saccharomyces cerevisiae, a Multinuclear Copper Ferroxidase Enzyme. J. Biol. Chem. 1998, 273 (36), 23274–23282. [PubMed: 9722559]

39. Stoll S; Schweiger A, EasySpin, a comprehensive software package for spectral simulation and analysis in EPR. J. Magn. Reson. 2006, 178 (1), 42–55. [PubMed: 16188474]

40. Frisch MJ; Trucks GW; Schlegel HB; Scuseria GE; Robb MA; Cheeseman JR; Scalmani G; Barone V; Petersson GA; Nakatsuji H; Li X; Caricato M; Marenich AV; Bloino J; Janesko BG; Gomperts R; Mennucci B; Hratchian HP; Ortiz JV; Izmaylov AF; Sonnenberg JL; Williams; Lipparini F; Egidi F; Goings J; Peng B; Petrone A; Henderson T; Ranasinghe D; Zakrzewski VG; Gao J; Rega N; Zheng G; Liang W; Hada M; Ehara M; Toyota K; Fukuda R; Hasegawa J; Ishida M; Nakajima T; Honda Y; Kitao O; Nakai H; Vreven T; Throssell K; Montgomery JA Jr.; Peralta JE; Ogliaro F; Bearpark MJ; Heyd JJ; Brothers EN; Kudin KN; Staroverov VN.; Keith TA; Kobayashi R; Normand J; Raghavachari K; Rendell AP; Burant JC; Iyengar SS; Tomasi J; Cossi M; Millam JM; Klene M; Adamo C; Cammi R; Ochterski JW; Martin RL; Morokuma K; Farkas O; Foresman JB; Fox DJ Gaussian 16Rev. B.01, Wallingford, CT, 2016.

41. Di Bilio AJ; Hill MG; Bonander N; Karlsson BG; Villahermosa RM; Malmström BG; Winkler JR; Gray HB, Reorganization Energy of Blue Copper: Effects of Temperature and Driving Force on the Rates of Electron Transfer in Ruthenium- and Osmium-Modified Azurins. J. Am. Chem. Soc. 1997, 119 (41), 9921–9922.

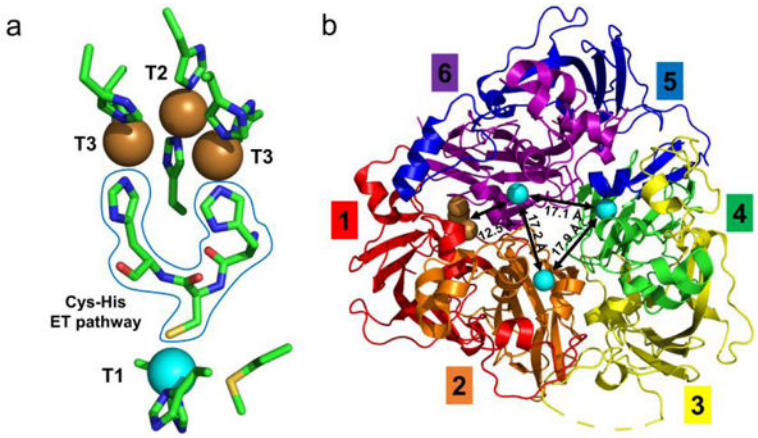

Figure 1.

(a) Crystal structure of the active site for O_2 reduction in Cp; (b) The overall organization of the Cp, showing the six domains (domains 1, 2, 3, 4, 5 and 6 in red, orange, yellow, green, blue and purple respectively) and the locations of the Cu binding sites (Cu atoms in the T1 Cu sites and the TNC in cyan and brown respectively). (PDB: 2J5W)

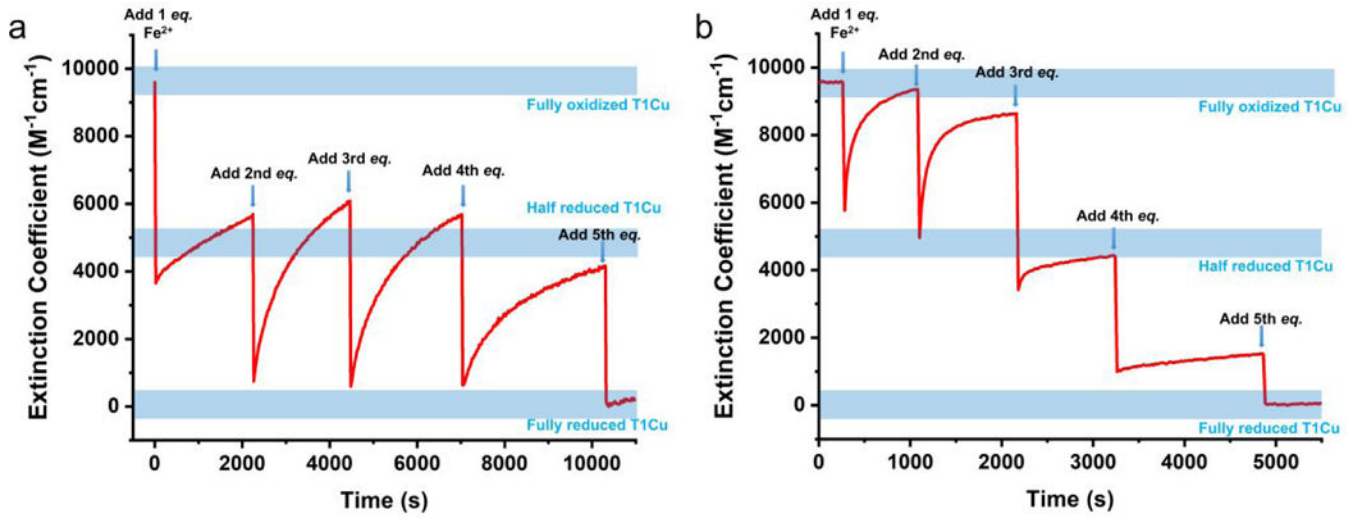

Figure 2.

Anaerobic reduction titrations of fully oxidized human Cp with Fe(II) monitored by absorption at 610 nm. Stoichiometric amount of Fe(II) from 10 mM $(NH_4)_2FeSO_4$ stock solution was added into ~ 50 μM Cp solution under stirring at room temperature. The number of the reduced T1 Cu was determined by ε_{610nm} = 4800 $M^{-1}cm^{-1}$ per T1 Cu site. (a) in MOPS pH7.0 buffer; (b) in MOPS pH7.0 buffer with 100 mM NaCl.

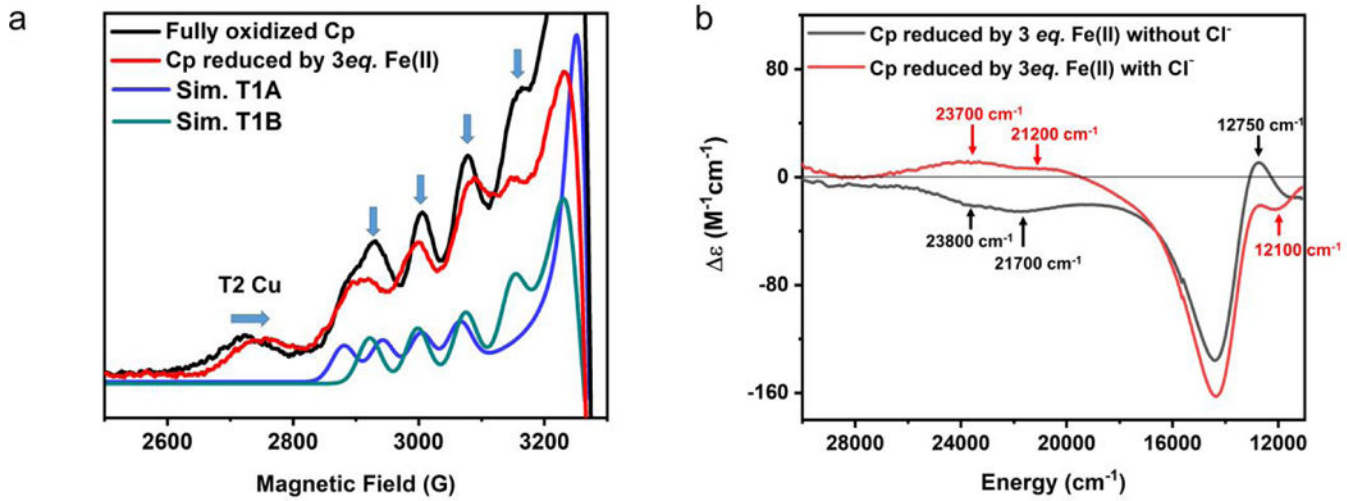

Figure 3.

Spectroscopic characterization of Cl^- binding to the partially reduced TNC. (a) EPR spectra of Cp and Cp reduced by 3 equivalents of Fe(II) in MOPS pH 7.0 with 100 mM NaCl and simulated EPR trace of the T1A and T1B Cu sites; (b) MCD spectra of Cp reduced by 3 equivalents of Fe(II) in MOPS pH7.0 buffer with and without 100 mM NaCl.

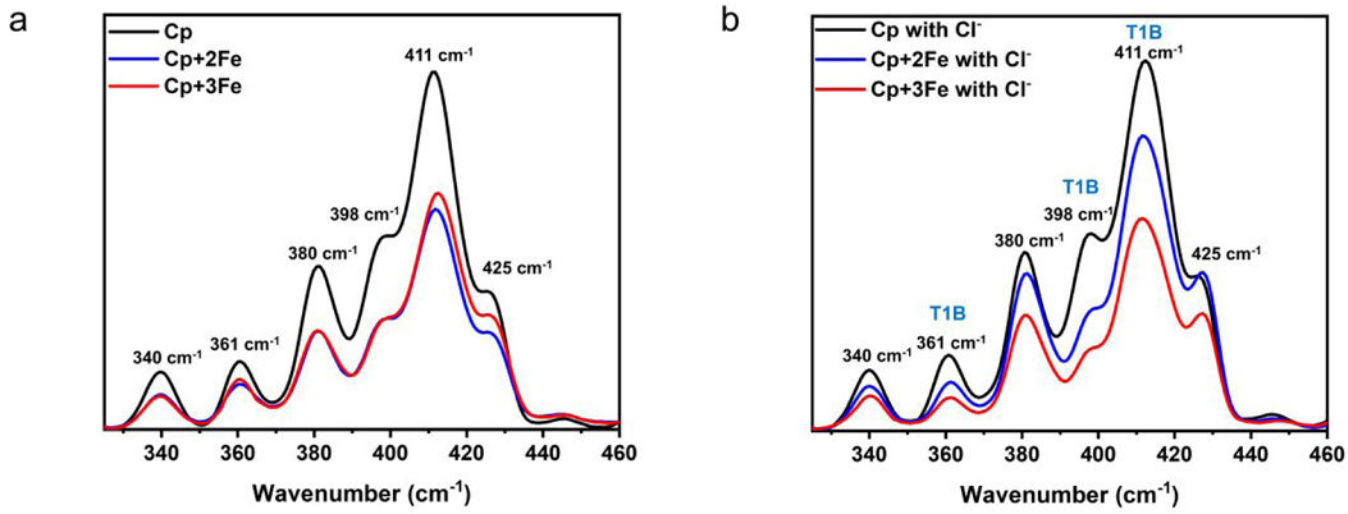

Figure 4.

rR spectra of Cp samples excited at 647.1 nm. (a) rR spectra of fully oxidized Cp, Cp reduced by 2 equivalent of Fe(II) and 3 equivalent of Fe(II) in MOPS pH7.0 buffer; (b) rR spectra of fully oxidized Cp, Cp reduced by 2 equivalent of Fe(II) and 3 equivalent of Fe(II) in MOPS pH7.0 buffer with 100 mM NaCl. All the rR samples were prepared with 0.2 mM Cp and the spectra were recorded for 20 minutes while rotating the sample to minimize photodecomposition. The intensities of rR spectra were normalized based on the ice peak at 228 cm^{-1}.

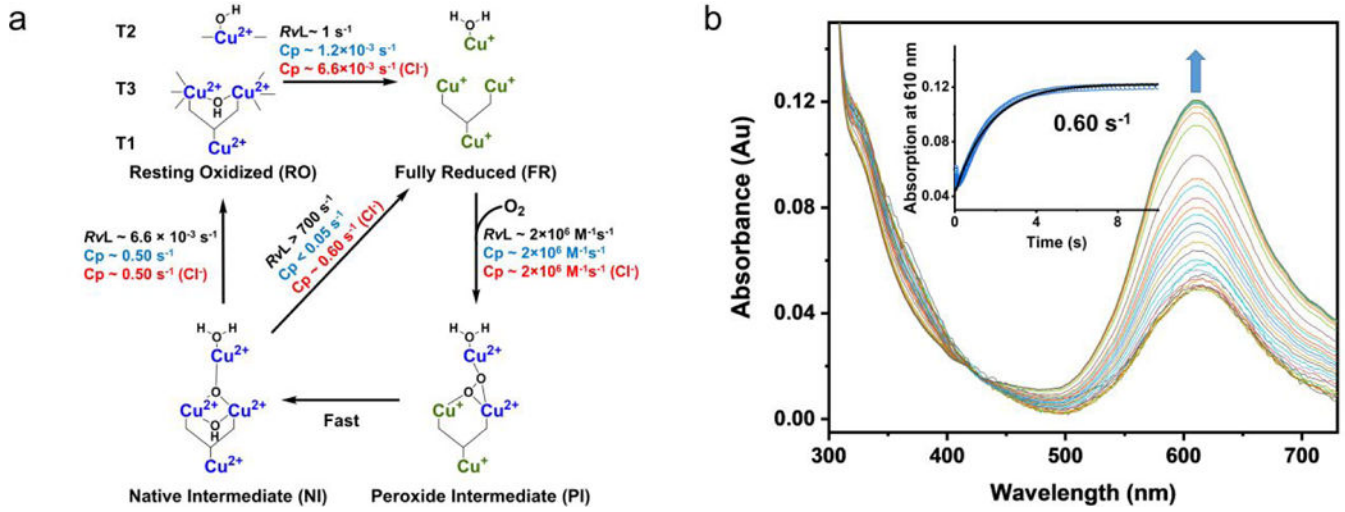

Figure 5.

Effect of Cl^- on Cp catalysis. (a) General mechanism of MCO; (b) Stopped-flow measurement of the IET between NI and reduced T1 Cu sites of Cp in the presence of 100 mM Cl^-. 50 μM of fully reduced Cp solution containing 50 μM Fe(II) was reacted with 1.3 mM O_2 dissolved in MOPS pH7.0 buffer with 100 mM NaCl at 4 °C. The IET rate was measured based on the reoxidation of the 610 nm band and fitted with first-order kinetics.

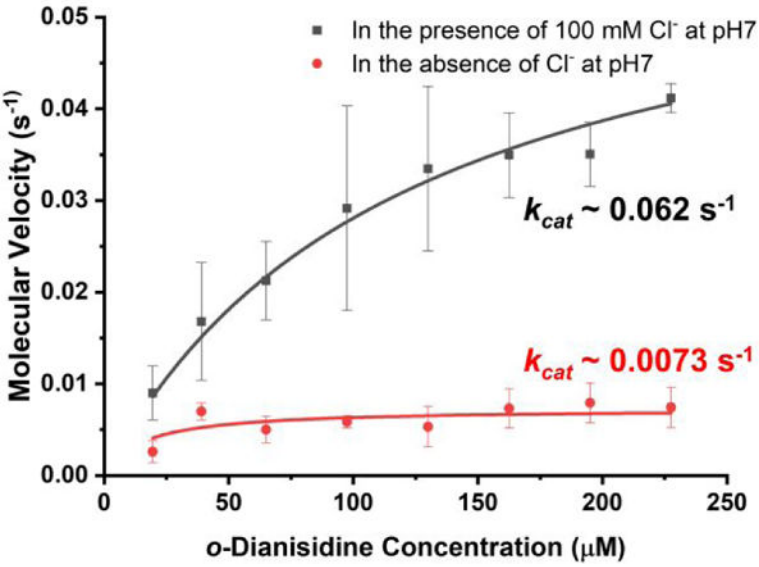

Figure 6.

The reaction rates were plotted versus the *o*-dianisidine concentration and subsequently analyzed by direct fitting to the Michaelis-Menten equation resulting k_{cat} ~ 0.062 s^{-1} and ~ 0.0073 s^{-1} with and without Cl^{-} at 25 °C respectively.

Table 1.

Reduction Potentials of the Cu sites in Human Cp

Cu sites	Potentials in the absence of Cl^- at pH7.0 (mV vs NHE)	Potentials in the presence of 100 mM NaCl at pH7.0 (mV vs NHE)
T1A Cu, T1B Cu	429, 429	392, 458
T2 Cu	394	332
T3 Cu	422	529